ARTICLE
Journal of Cellular Biochemistry 111:1401–1412 (2010)

Journal of Cellular Biochemistry

Identification of New Modulators and Protein Alterations in Non-Apoptotic Programmed Cell Death

Sabina Sperandio,[1,2] Karen S. Poksay,[1] Birgit Schilling,[1] Danielle Crippen,[1] Bradford W. Gibson,[1] and Dale E. Bredesen[1,3*]

[1]*Buck Institute for Age Research, Novato, California 94945*
[2]*Center for Cancer Therapeutics, Ottawa Hospital Research Institute, Ottawa, Ontario, Canada*
[3]*Department of Neurology, University of California-San Francisco, San Francisco, California*

ABSTRACT

This study describes the first proteomic analysis of paraptosis—a non-apoptotic form of programmed cell death. As with apoptosis, the first description of paraptosis was based on morphological criteria. Since there are no known markers for paraptosis, the purpose of this study was to dissect changes in the proteome profile occurring during paraptosis. Using one- and two-dimensional SDS–PAGE, Western analysis, and mass spectrometry, we show that during paraptosis, alterations occur mainly in cytoskeletal proteins, signal transduction proteins, mitochondrial proteins, and some metabolic proteins. We also report the identification of: (1) a paraptosis inhibitor, phosphatidylethanolamine binding protein (PEBP-1), and (2) a candidate mediator of paraptosis, prohibitin. Identification of specific paraptotic changes will ultimately lead to tools to detect this type of programmed cell death in in vivo systems and allow for its further characterization. J. Cell. Biochem. 111: 1401–1412, 2010.

KEY WORDS: PARAPTOSIS; PROTEOMICS; INSULIN-LIKE GROWTH FACTOR I RECEPTOR

Programmed cell death (pcd) is an essential process for the development and maintenance of multicellular organisms. During development, pcd participates in morphogenesis, sexual differentiation, and the complex processes of trophic factor-mediated selection necessary for the development of the nervous and immune systems. In the adult, pcd is fundamental for tissue homeostasis and for defense against infections. Conversely, pcd dysregulation is implicated in the pathogenesis of several diseases such as cancer, neurodegenerative, and autoimmune diseases. Though pcd has been reported in prokaryotic organisms, it is not clear whether this is essential to the species' survival [see Ameisen, 2002 for a review].

At least three types of naturally occurring pcd have been described based on their morphological features [Clarke, 1990]. Type 1 cell death, also called nuclear cell death, and more recently apoptosis, is the most prominent type of pcd that occurs during mammalian development. Type 2 cell death, or lysosomal cell death, also described as autophagic cell death, is observable during the removal of vestigial organs such as the involution of salivary glands in insects. Type 3, or cytoplasmic cell death, has been described in the developing nervous system.

Apoptosis is by far the most well-characterized form of pcd, with over 100,000 publications on this subject to date. Its study has been accelerated during the past two decades following the identification, in the nematode *Caenorhabditis elegans*, of the genetic components of apoptosis [Yuan and Horvitz, 1992; Yuan et al., 1993]. A class of proteases called caspases (cysteine aspartyl-specific proteases), with high specificity of recognition and cleavage after specific aspartate residues, was found to play a major role in the execution of this type of cell demise [Yuan et al., 1993].

The morphological features of apoptosis are readily recognizable. These include: chromatin condensation and nuclear fragmentation, plasma membrane blebbing, and cell shrinkage, ultimately leading to the formation of cellular fragmentation products called apoptotic bodies. A variety of highly sophisticated methods are now available for the detection of apoptosis, taking advantage of unique apoptotic mechanisms such as the specificity of cleavage by caspases and the typical periodicity of DNA fragmentation.

Sabina Sperandio and Karen S. Poksay contributed equally to this work.
Grant sponsor: National Institutes of Health; Grant number: AG12282.
*Correspondence to: Dale E. Bredesen, Buck Institute for Age Research, 8001 Redwood Blvd., Novato, CA 94945.
E-mail: dbredesen@buckinstitute.org
Received 10 August 2009; Accepted 24 August 2010 • DOI 10.1002/jcb.22870 • © 2010 Wiley-Liss, Inc.
Published online 9 September 2010 in Wiley Online Library (wileyonlinelibrary.com).

Because of its widespread occurrence during development as well as its presence in experimental models of cellular insult, along with the availability of many specific markers, apoptosis has often been equated with pcd. However, due in part to the lack of specific markers, the incidence of other, non-apoptotic forms of pcd has not been thoroughly investigated and may thus have been underestimated. These other forms of pcd may help explain the cell death observed in some pathological conditions, such as excitotoxicity, ischemia, and neurodegeneration, in which not all cell death appears to occur via apoptosis.

We have previously reported that a form of pcd morphologically very similar to that of type 3 can be induced in mammalian cells following the expression of the intracytoplasmic domain of the insulin-like growth factor I receptor (IGF-IR-IC) [Sperandio et al., 2000]. This cell death was prevented by inhibitors of protein synthesis and transcription, indicating that it is programmatic in nature. We dubbed this form of pcd ''paraptosis.'' The main feature of paraptosis consists of extensive cytoplasmic vacuolation without significant cell membrane blebbing, nuclear shrinkage, or pyknosis. Apoptosis inhibitors are ineffective in preventing paraptosis, indicating a distinct biochemical process. Kinetically, paraptosis is slower than apoptosis: in an experiment that compared the rate of cell death induced by the transfection of IGF-IR-IC and the apoptotic protein Bax, we found that, while in the Bax sample the majority of cell death occurred within 24 h, the incidence of cell death in the IGF-IR-IC sample was distributed within at least 5 days, though with a peak at 48 h [Sperandio and de Belle, 2008].

Paraptosis is also insensitive to autophagic cell death inhibitors such as 3-methyladenine; however, to date the most defining feature that differentiates it from autophagic cell death is the absence of autophagic vacuoles in paraptosis.

Subsequently, we reported that the binding of the peptide neurotransmitter substance P to its receptor, the neurokinin-1 receptor, also induces a non-apoptotic form of pcd with some similarities to paraptosis in morphology, caspase independence, and requirement for gene transcription and translation [Castro-Obregon et al., 2002]. However, substance P-induced pcd also bears some similarities to autophagic pcd [Castro-Obregon et al., 2002]. Since then, other groups have reported observing forms of cell death similar to paraptosis, including the response to: (1) the overexpression of the TAJ/TROY tumor necrosis factor receptor in 293T cells [Wang et al., 2004b], (2) intracellular acidification in cerebellar granule neurons [Schneider et al., 2004], (3) M-CSF transduction or transfection in U251MG glioma cells or T9-C2 glioma cells [Jadus et al., 2003], and (4) EGF in somato-lactotrope pituitary cells [Fombonne et al., 2006].

In further studies, we reported that paraptosis induced by the IGF-IR is the result of a constitutive positive signaling through the receptor, and that at least two signal transduction pathways participate in the execution of paraptosis, the MAPK and the JNK pathways [Sperandio et al., 2004]. Consequently, we were able to prevent paraptosis with the use of specific inhibitors for these protein kinases. We also identified the first natural inhibitor of paraptosis in AIP1/Alix, a protein cloned from its interaction with ALG-2, a calcium-binding protein involved in T-cell receptor-induced cell death. Perhaps relevant to this finding, expression of the C-terminal region of AIP1 has been shown to induce the formation of intracellular vacuoles through its interaction with endophilins [Chatellard-Causse et al., 2002].

With the purpose of characterizing the molecular changes occurring during paraptosis, we performed a proteomic analysis following the transfection of IGF-IR-IC into 293T cells. From this differential profiling study, we report that during paraptosis, quantitative and/or qualitative alterations occur in several proteins including signal transduction proteins, structural proteins, mitochondrial proteins, and proteins related to cellular metabolism. Changes in alpha- and beta-tubulins appear directly related to microtubule disorganization and the consequent perturbation of the cytoskeleton in paraptotic cells. We also describe here the finding of a natural inhibitor for paraptosis, PEBP, as well as linking the observed induction of prohibitin to a possible functional role in paraptosis.

RESULTS

In order to identify molecular changes occurring during paraptosis, the proteome profiles of extracts from 293T cells undergoing paraptosis were compared to those of controls. We induced paraptosis by transiently transfecting 293T cells with the construct pcDNA3-IGF-IR-IC (Fig. 1B) previously described: the intracytoplasmic domain of the IGF-IR targeted to the plasma membrane by the addition of the Src myristylation motif [Sperandio et al., 2000]. We consistently obtain transfection efficiencies of 70–90% with this cell line independent of the construct used; transfections of 80% or greater efficiency were used for this series of experiments. The cells were collected 48 h following transfection, at which time there is a peak in the rate of cell death. We then performed fractionation of the lysates by differential centrifugation to obtain protein enrichment in specific subcellular compartments. The following samples were prepared: P20 (pellet of the 20,000*g* spin), containing heavy membranes including mitochondria and lysosomes; P400 (pellet of the 436,000*g* spin) containing light membranes, including endosomes and Golgi; and S400 (supernatant of the 436,000*g* spin), enriched in cytosolic proteins. In addition, some experiments were performed using lower speed 100,000*g* centrifugations (S100). Equal amounts of protein from control or paraptotic extracts were subjected to two-dimensional (2D) SDS–PAGE, and gels were stained with colloidal Coomassie and/or Sypro Ruby. Representative 2D SDS–PAGE gels of S100 cell extracts containing several proteins of interest are shown in Figure 2A,B. Protein spots of different intensity between the two conditions were excised from the gel and analyzed by MALDI mass spectrometry to obtain peptide mass fingerprint (PMF) data, and in some cases, by ESI-MS/MS to obtain peptide sequence data. MALDI-MS and ESI-MS/MS spectra are shown in Figure 3 for two proteins whose levels were found to be altered in this study: (A) PEBP-1 and (B) prohibitin.

In a parallel pilot study, we performed DIGE (2D fluorescence difference gel electrophoresis) analysis of P20 mitochondrial extracts. With this approach, in which the differences in abundance of proteins are compared within the same gel, one protein we

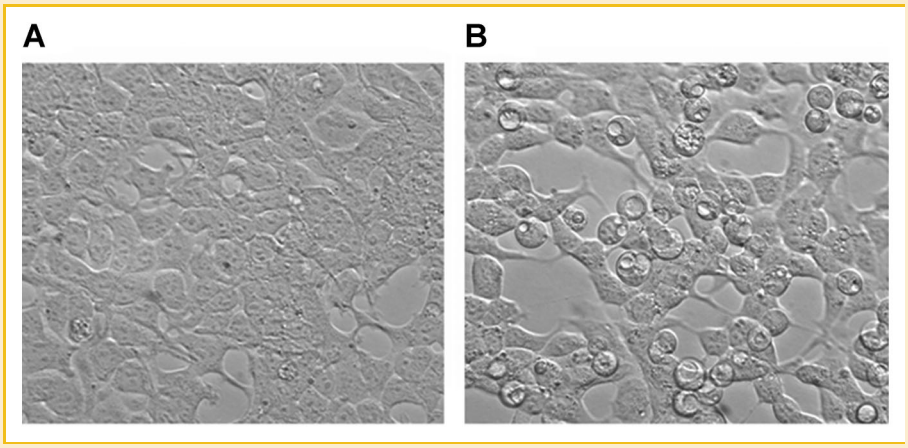

Fig. 1. Cellular morphology of 293T cells undergoing paraptosis. Light microscopy images of 293T cells 48 h after transfection with either control (pcDNA3) (A) or IGF-IR-IC constructs (B). Marked morphological changes are obvious in paraptotic cells including cell rounding and pronounced cytoplasmic vacuoles.

identified at a higher abundance in paraptotic cells, compared to control, was the mitochondrial protein prohibitin.

To confirm 2D SDS–PAGE findings and measure the changes in abundance of various proteins, one-dimensional (1D) SDS–PAGE Western blot analyses and densitometry were performed. Equal protein amounts from control and paraptotic 293T cell extracts were run on 1D SDS–PAGE. Figure 4 shows representative Western blots for proteins found to be consistently altered in cells undergoing paraptotic cell death. Table I summarizes the proteins found to change consistently in abundance in two or more independent experiments. The average fold changes in protein abundance were determined by 1D SDS–PAGE Western blot densitometry.

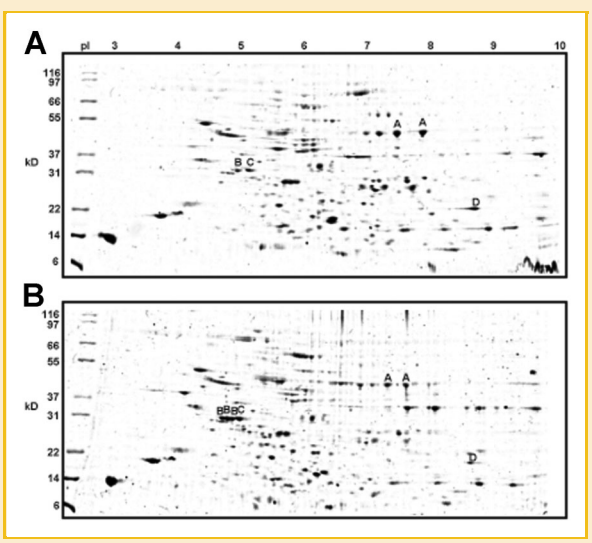

Fig. 2. 2D SDS–PAGE gel separation of 293T cell S100 cytosolic extracts. A: control = transfection with pcDNA3, and (B) paraptosis = transfection with pcDNA3-IGF-IR-IC. Gels were stained with colloidal Coomassie fast stain, and differences in the levels of these relatively abundant proteins were analyzed. Proteins shown here are: A = enolase-1, alpha; B = 14-3-3, epsilon; C = tropomyosin-3, cytoskeletal; D = phosphatidylethanolamine binding protein-1 (PEBP-1). Some of the changes observed in this fractionation are: decreases in the levels of enolase-1, alpha and phosphatidylethanolamine binding protein (PEBP) and an increase in the level of 14-3-3 isoforms.

Interestingly, among the proteins confirmed by Western blot to be altered in paraptosis, three were structural proteins, namely α-tubulin, β-tubulin, and tropomyosin (Fig. 4). The cytoskeletal proteins α- and β-tubulin are the major building blocks of microtubules, one of the main components of the cytoskeleton. Besides providing the cell's structural support, microtubules participate in a variety of cellular movements such as organellar transport, cell locomotion, and chromosome separation during mitosis. Tropomyosin is a major component of the thin filaments in vertebrate striated and smooth muscle where it participates in the regulation of the contractile process. In non-muscle cells, tropomyosin is found associated with the cytoskeleton and the actin-based motor system [Perry, 2001]. As shown in Figure 4 and in Table I, we found that in cells undergoing paraptosis, α-tubulin and tropomyosin were both more abundant in the light membrane/organelle (P400) fractions and less abundant in the cytosol and in the P20 fraction (tropomyosin); β-tubulin levels were found to be decreased overall from control in the paraptotic fractions (Fig. 4). The altered relative abundance found in subcellular fractions of cells undergoing paraptosis is suggestive of an intracellular redistribution of these proteins during paraptosis. To confirm this hypothesis, we performed experiments of immunofluorescence followed by confocal imaging for these proteins. For both α- and β-tubulin, we observed a different degree of alteration of both protein levels and distribution within the population of cells transfected with IGF-IR-IC (Fig. 5). Some paraptotic cells showed a major alteration of the microtubular network and peripheralization of the tubulin staining, while others showed a profound decrease in both tubulins levels. The major difference observed in the tropomyosin staining was a marked peripheralization in paraptotic cells (Fig. 5).

Another protein found consistently to be less abundant in paraptotic cells is PEBP. Also known as Raf kinase inhibitor protein (RKIP) PEBP is a multifunctional protein whose proposed roles include the biogenesis of the hippocampal cholinergic neurosti-

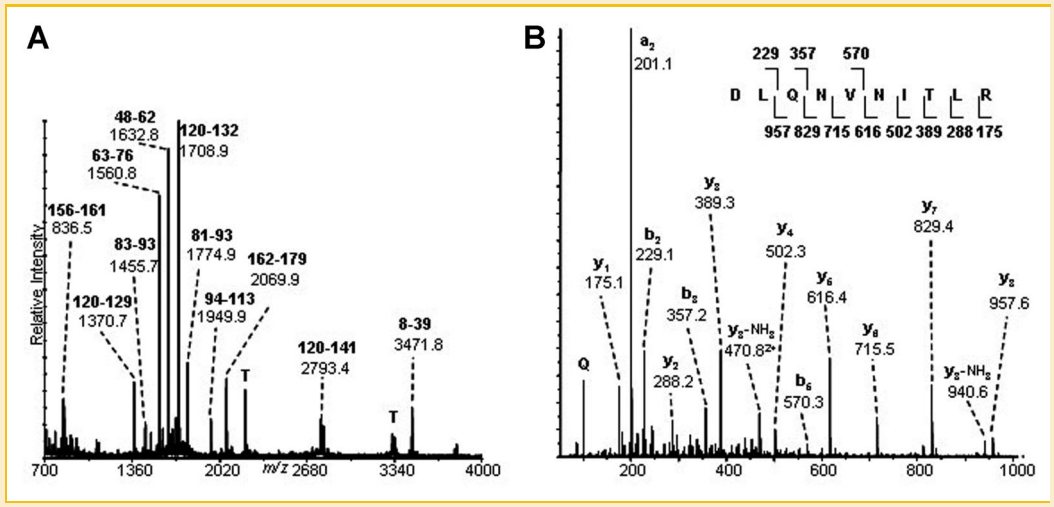

Fig. 3. Mass spectrometry analysis for PEBP and prohibitin. A: MALDI-TOF MS peptide mass fingerprint spectrum displaying molecular ions of peptides obtained after in-gel trypsin digestion of the protein spot phosphatidylethanolamine binding protein-1 (PEBP-1). Sixteen peptide mass fingerprints were identified as peptides resulting from this tryptic digestion. The observed masses are labeled and annotated with starting and ending amino acids. Overall, a protein sequence coverage of 81% was observed for this 21 kDa protein/p*I* 7.0 (151/187 amino acids). B: ESI-MS/MS spectrum of peptide DLQNVNITLR (residues D-84 to R-93) obtained after tryptic digestion of the protein spot prohibitin (30 kDa/p*I* 5.6). The molecular ion $[M+2H]^{2+}$ at *m/z* 593.31^{2+} ($M_{exp} = 1184.63$, $M_{calc} = 1184.65$) was selected for collision-induced dissociation (CID). A nearly complete series of *y*-fragment ions and several *b*-fragment ions were observed.

mulating peptide (HCNP) [Ojika et al., 2000], inhibition of the Raf kinase [Yeung et al., 1999], inhibition of apoptosis [Wang et al., 2004a], and inhibition of serine proteases [Hengst et al., 2001]. Figure 3A shows a MALDI-MS PMF clearly identifying a spot on a 2D gel from a P400 extract as PEBP. In this study, we found decreased levels of PEBP in paraptotic samples as compared to control (Figs. 2 and 4) in all of the subcellular fractions analyzed.

We previously reported that paraptosis induced by the IGF-IR requires signaling through the MAPK and JNK pathways [Sperandio et al., 2004], and therefore downregulation of PEBP or other kinase inhibitors might be critical to allow sufficient levels of active MAPK and JNK to induce cell death. In support of this notion, we found here that PEBP cotransfection with IGF-IR-IC prevents the cell death induced by the IGF-IR-IC in 293T cells, indicating that this small protein can function as a paraptosis, as well as an apoptosis, inhibitor (Fig. 6). However, Western blot analysis reveals that cotransfection with PEBP prevents phosphorylation (and activation) of JNK1 but does not decrease the levels of phospho-MAPK induced by transfection of the IGF-IR-IC (Fig. 6). These results are consistent with our previous report demonstrating that specific downregulation of JNK1 by means of antisense oligos prevents paraptosis [Sperandio et al., 2004]. To further assess whether changes in the subcellular distribution of the remaining PEBP occur in paraptosis, we performed immunofluorescence staining for PEBP followed by confocal imaging of 293T cells transfected with IGF-IR-IC. We observed a cytoplasmic staining with a punctate appearance perhaps

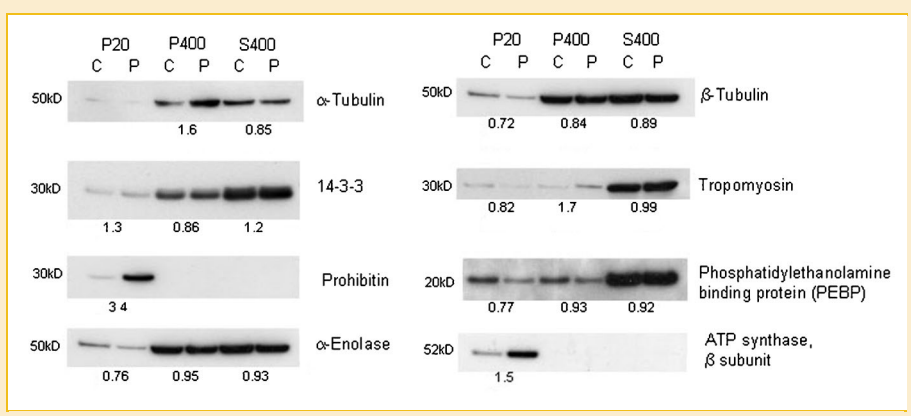

Fig. 4. Western blot analysis of 293T cell extracts from control or paraptotic cells. Relative protein abundance and intracellular distribution in representative 1D SDS–PAGE Western blots of control (C: pcDNA3) and paraptotic (P: pcDNA3-IGF-IR-IC) 293T cell fractionations. P20 represents heavy membranes, P400 represents light membranes, and S400 represents the cytosolic fraction. Fold change values listed were derived from densitometric analysis of 2–5 experiments and are expressed as the mean of the quotient of the paraptotic density divided by the control density; a value greater than 1 represents an increased level of the protein in paraptosis.

TABLE I. Protein Abundance Alterations During Paraptosis: Identification by 2D SDS–PAGE and Mass Spectrometry and Quantification by 1D SDS–PAGE Western Blot Densitometry

Protein	Function	1D SDS–PAGE change from control[a] subcellular fractions			Acc. #[b]	Obs. MW/p*I*	Theor. MW/p*I*	Seq. cov. (%)[c]	Mascot score (exp. value)[d]	No. try. pep.[e]
		P20	P400	S400						
14-3-3, epsilon	Signal transduction	1.3 (1.1–1.5), n = 3	0.86 (0.74–0.98), n = 2	1.2 (1.1–1.2), n = 2	P62258	29/5	29/4.6	49	102 (8.9E−007)	12
ATP synthase, beta chain	Energy metabolism	1.5 (1.1–2.6), n = 4			P06576	53/5.5	57/5.3	79	191 (1.1E−015)	29
Enolase, alpha[f]	Glycolytic enzyme	0.76 (0.72–0.79), n = 2	0.95 (0.81–1.1), n = 4	0.93 (0.84–1.1), n = 4	P06733	50/7	47/7	68	192 (8.9E−016)	27
Phosphatidylethanolamine binding protein-1 (PEBP-1)[g]	Signal transduction	0.77 (0.61–0.90), n = 4	0.93 (0.81–1.1), n = 4	0.92 (0.84–0.95), n = 4	P30086	25/8	21/7	81	146 (3.6E−011)	16
Prohibitin[h]	Cell-cycle tumor sup.	3.4 (1.1–6.1), n = 5			P35232	30/5.5	30/5.6	53	604 (1.1E−064)[i]	14
Tropomyosin-3	Cytoskeleton	0.82 (0.68–0.96), n = 2	1.7 (1.3–2.1), n = 2	0.99 (0.87–1.1), n = 2	P06753	30/5	33/4.7	43	146 (3.6E−011)	21
Tubulin, alpha[i]	Cytoskeleton		1.6 (1.3–1.9), n = 2	0.85 (0.81–0.89), n = 2	P68363	52/4	51/4.9	52	119 (1.8E−008)	22
Tubulin, beta[j]	Cytoskeleton	0.72 (0.54–0.83), n = 4	0.84 (0.55–0.89), n = 5	0.89 (0.70–1.2), n = 4	Q9H4B7	50/6	50/5.1		[j]	

Protein abundance alterations in subcellular fractions during paraptosis. Differences in abundance were determined by 1D SDS–PAGE Western blot densitometry and are expressed as average fold changes (with range). Proteins were identified on 2D SDS–PAGE, and detailed mass spectrometric information is also shown. The observed molecular weights and p*I* values are compared with the theoretical values, and protein sequence coverage is reported. The number of observed tryptic peptides provides a qualitative confidence level, but more important are the statistical scores (''MOWSE Score'') and expectation values for PMF and MS/MS sequence data searches generated by the database search engine Mascot [Perkins et al., 1999].

[a]Abundance changes from 1D SDS–PAGE were derived using Western blot densitometry. Values represent the mean (with range) of the quotient of the paraptotic density divided by the control density; values >1 represent an increased level of the protein in paraptosis. If box is blank, no protein was detected in this fraction.

[b]SwissProt protein accession numbers.

[c]Protein sequence coverage as observed by mass spectrometry.

[d]Mascot database search engine scores and expectation values for peptide mass fingerprint data from MALDI-MS were obtained from 2D SDS–PAGE.

[e]Number of tryptic peptides as observed by mass spectrometry provides a qualitative confidence level.

[f]Also decreased 0.3-fold in paraptotic S100 cytosolic extract as analyzed on 2D SDS–PAGE with PDQuest.

[g]Also decreased 0.7-fold in paraptotic S100 cytosolic extract as analyzed on 2D SDS–PAGE with PDQuest.

[h]Also increased 1.6-fold in paraptotic P20 membrane extract as analyzed by DIGE. Protein identification by nano-LC–ESI-MS/MS.

[i]Also decreased 0.5-fold in paraptotic S100 cytosolic extract as analyzed on 2D SDS–PAGE with PDQuest.

[j]Analyzed because of changes in morphology during paraptosis. No mass spectrometric analysis performed.

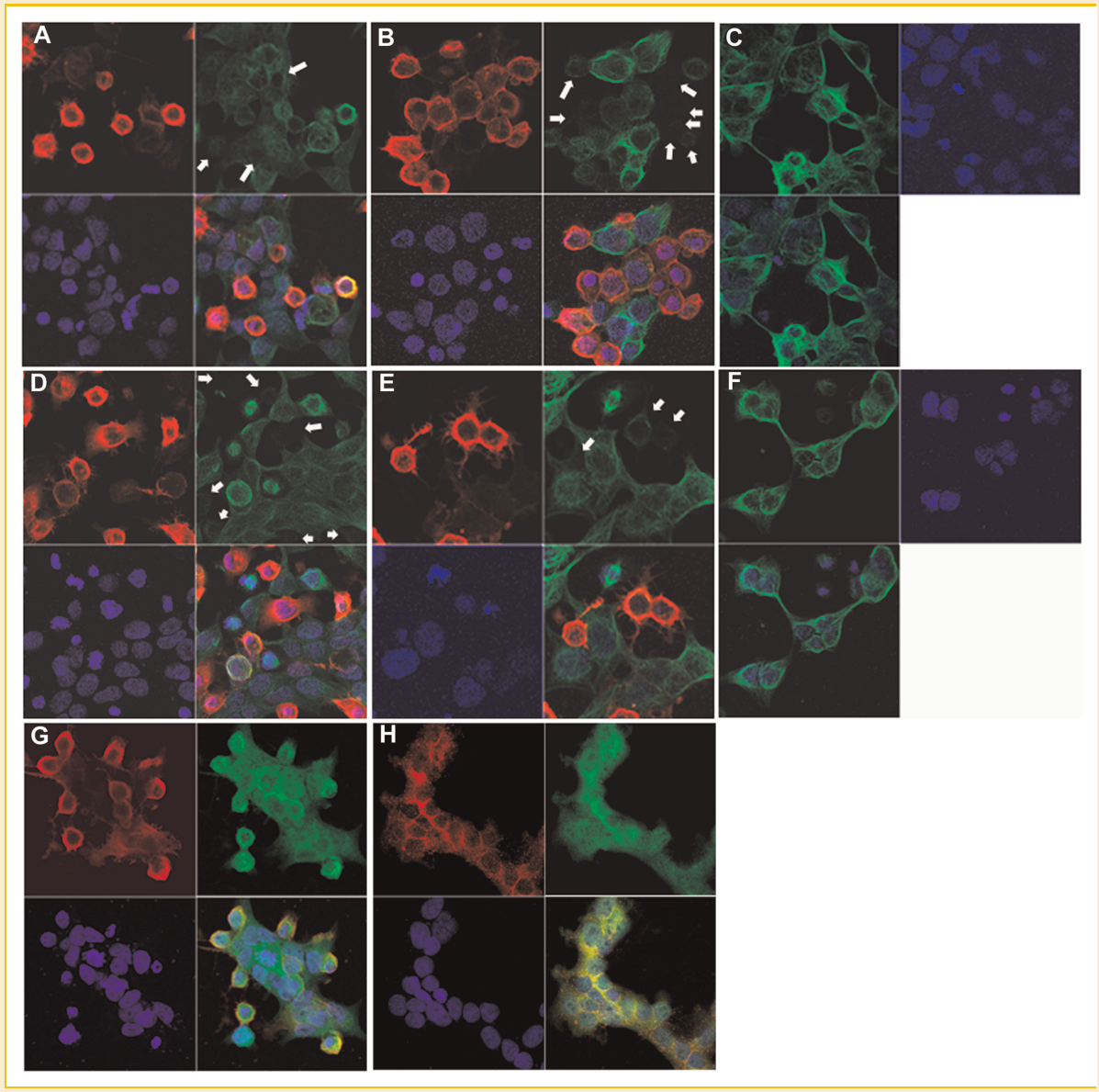

Fig. 5. Confocal imaging following immunofluorescence staining for α- and β-tubulins and tropomyosin in 293T cells. Cells were transfected with pcDNA3-IGF-IR-IC in A, B, D, E, and G or pcDNA3 in C, F, and H. Staining was performed 24 h following transfection. In A, B, and C, green = α-tubulin, red = IGF-IR-IC, and blue = DAPI (nuclear counterstaining). In D, E, and F, green = β-tubulin, red = IGF-IR-IC, and blue = DAPI. In G and H, green = tropomyosin, red = IGF-IR-IC, and blue = DAPI. White arrows indicate cells with reduced or absent staining for α- or β-tubulin. The images are representative from multiple experiments.

deriving from organellar membranes associated PEBP. Though we could clearly appreciate a decrease in the staining intensity, there was no obvious alteration in the subcellular distribution of PEBP in paraptotic cells (Fig. 6C).

Two mitochondrial proteins were found to be altered in paraptosis; the β-subunit of ATP-synthase and prohibitin. ATP synthase is a ubiquitous multisubunit enzyme that catalyzes the synthesis of ATP from ADP and Pi and is located in the inner mitochondrial membrane as part of the oxidative phosphorylation complex V. We found the ATP synthase β-subunit to be more abundant in P20 mitochondrial fractions of paraptotic cells than in controls (Fig. 4). Synthesis of ATP is necessary for the execution of apoptotic pcd, and the inhibition of protein synthesis upon administration of apoptotic stimuli results in necrosis or uncontrolled cell death. Here we found increased levels of an enzyme fundamentally involved in oxidative phosphorylation, which could indicate a need for ATP production for the execution of paraptosis. In support of this hypothesis, we found that specific inhibition of the F_1F_0 ATPase with oligomycin B prevents the appearance of the typical paraptotic morphology, cell rounding, and formation of cytoplasmic vacuoles, indicating that during paraptosis these are active processes that require energy (data not shown).

Prohibitin is another inner mitochondrial membrane protein with proposed roles in cell-cycle regulation, replicative senescence,

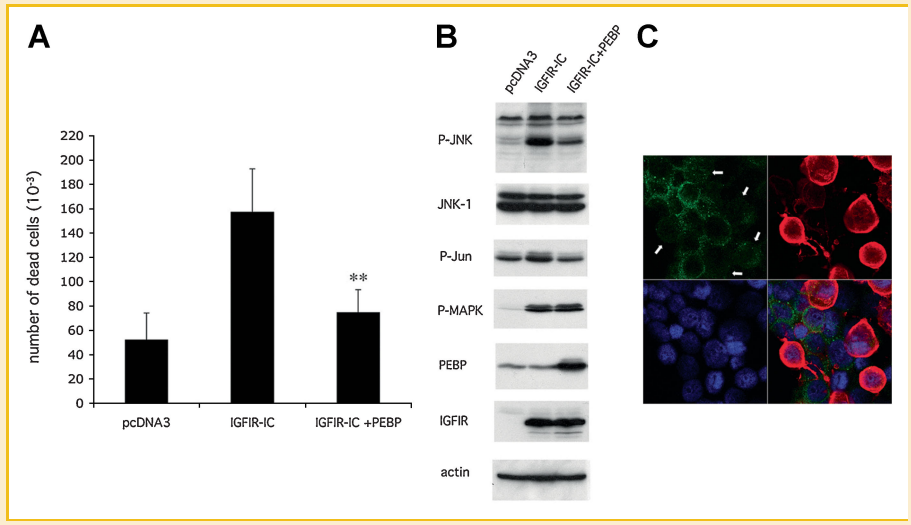

Fig. 6. Phosphotidylethanolamine binding protein (PEBP) is an inhibitor of paraptosis. A: 293T cells were transfected with IGF-IR-IC either alone or in combination with PEBP, and cell death was measured after 48 h. The error bars represent the SD of six independent experiments. The asterisks denote a highly statistically significant difference from IGF-IR-IC as assessed by Student's *t*-test ($P < 0.0046$). B: Western blot analysis on equal amounts of cell lysates from 293T cells transfected with IGF-IR-IC with or without a construct expressing PEBP. C: PEBP immunofluorescence staining followed by 60× confocal imaging of 293T cells 48 h after transfection with IGF-IR-IC. Green = α-PEBP, red = α-IGF-IR, blue = DAPI.

cellular immortalization, and tumor suppression. We initially identified prohibitin by MALDI-MS in our DIGE analysis of P20 mitochondrial extracts, where we found it increased 1.6-fold over control during paraptosis. We then confirmed the identity of this protein by subjecting the tryptic digestion mixture to ESI-MS/MS (Fig. 3B). From 1D SDS–PAGE Western blotting experiments, prohibitin levels in paraptotic mitochondrial P20 extracts were increased an average of 3.4-fold over control (Fig. 4).

Higher levels of prohibitin in cells undergoing paraptosis were also demonstrated by immunofluorescence staining of cells undergoing paraptosis, compared to both control and ER-stress induced apoptosis (Fig. 7). Rounded paraptotic cells exhibiting increased levels of prohibitin also present a more intense and altered mitochondrial staining (Mitotracker Red) that appears condensed in certain areas, suggesting alteration/reorganization of the mitochondrial network. Thompson et al. [2001] speculated that prohibitin expression may be indicative of mitochondrial destabilization during apoptotic events. Because prohibitin levels were found to be increased in paraptotic cell extracts as compared to controls, and because this protein is known to function as a tumor suppressor, we tested whether prohibitin could reproduce paraptosis in vivo. Following overexpression of prohibitin in 293T cells, the cell death we observed more closely resembled apoptosis than paraptosis. We found that prohibitin could in fact induce cell death, but that this could be prevented by caspase inhibitors (Fig. 8). However, when prohibitin was coexpressed with IGF-IR-IC, there was a synergistic effect on the non-apoptotic cell death. Upon treatment with the caspase inhibitor z-VAD.fmk, only the cell death induced by prohibitin alone was inhibited, while in the cotransfection, cell death was greater than in the z-VAD.fmk IGF-IR-IC sample alone. In conclusion, it appears that when increased levels of prohibitin are associated with a paraptotic stimulus such as expression of IGF-IR-IC, prohibitin can contribute to a cell death that is not inhibitable by caspase inhibitors. These results suggest that the increased prohibitin levels that we observe could play a functional role in the execution of paraptosis.

DISCUSSION

In this study, we report the first proteomic analysis of one type of non-apoptotic pcd, paraptosis [Sperandio et al., 2000, 2004]. Despite the fact that the approach we took could arguably be limited by protein solubilization, relative abundance, staining, and MS detection sensitivity, proteomic analyses have previously been successfully applied to studies of apoptotic cell death [Gerner et al., 2000; Thiede et al., 2001]. The mechanism of protein regulation—transcriptional or post-transcriptional—was not determined here, only the relative abundance of each individual protein candidate.

We found changes in abundance, or subcellular distribution, in members of at least four classes of proteins: structural proteins, signal transduction proteins, proteins involved in cellular metabolism, and mitochondrial proteins. The greatest changes in protein abundance were found in the two mitochondrial proteins, prohibitin and ATP-synthase-β subunit, indicating a previously unsuspected mitochondrial involvement in this cell death process. This study did not provide evidence of the involvement of proteolytic cleavage in paraptosis, although this could be due at least in part to sensitivity factors in detecting the appearance of protein fragments.

It is not surprising that we found alterations of some cytoskeletal proteins. In fact, during paraptosis, a major structural rearrangement is noticeable almost immediately upon light microscopic observation: the cells become rounded and the cytoplasm is reorganized by the appearance of pronounced vacuolation. Several

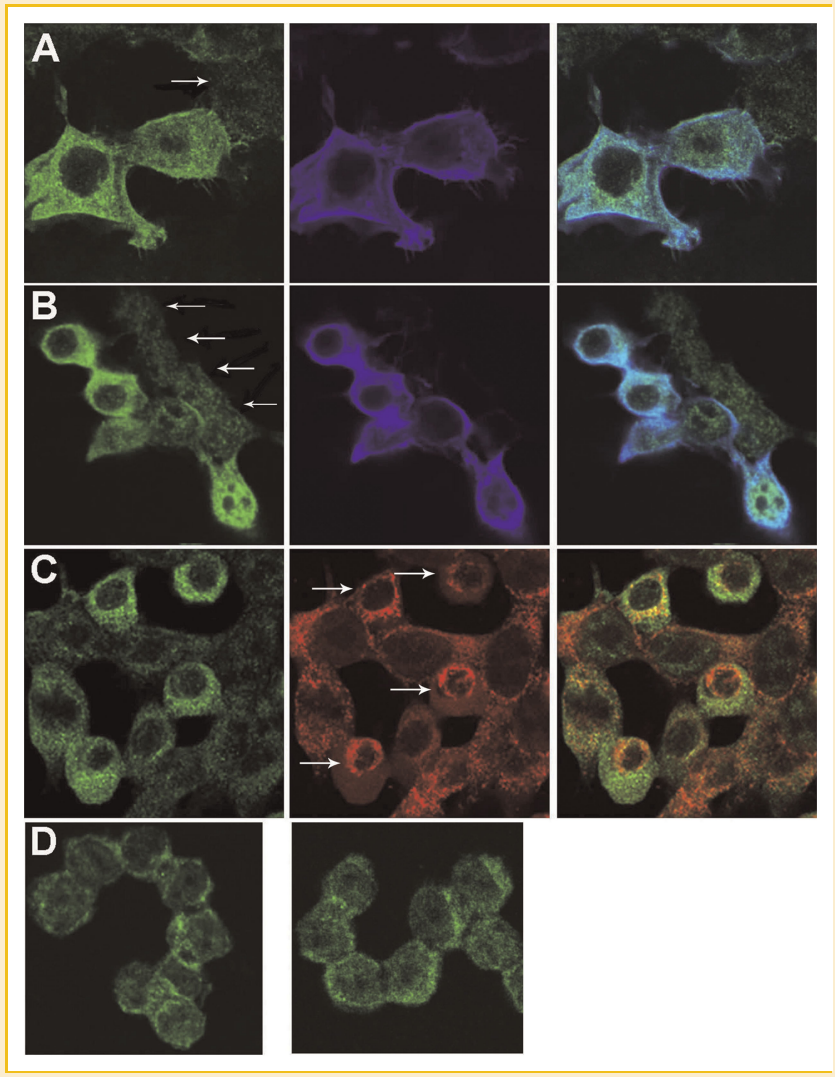

Fig. 7. Confocal imaging following immunofluorescence staining for prohibitin in 293T cells. A: 15 h IGF-IR-IC transfection: prohibitin (green) levels are higher in IGF-IR-IC transfected cells (blue) than in untransfected cells (arrow). Merge shown on right. B: 22 h IGF-IR-IC transfection: in addition to increased prohibitin (green) levels versus untransfected cells (arrows), cells are becoming rounded. C: Mitotracker Deep Red staining in 22 h IGF-IR-IC transfection: in transfected (rounded) cells, prohibitin (green) shows an intense cytoplasmic staining but also appears localized (yellow) to the mitochondria (red). In addition, Mitotracker staining appears more robust and condensed in cells exhibiting increased levels of prohibitin (arrows), indicating an alteration/reorganization of the mitochondrial network. D: Thapsigargin (TG) treatment (1 μM, 48 h): prohibitin (green) staining is less robust in cells undergoing apoptosis (D) than in those undergoing paraptosis (A,B,C). The images are representative from multiple experiments.

cytoskeletal and structure-related proteins such as actin, fodrin, and keratins, among others, have been found to be substrates of caspases in apoptotic cell death [Fischer et al., 2003]. The cleavage and inactivation (or otherwise alteration) of such proteins is presumed to allow for the cell shrinkage and membrane blebbing characteristic of apoptosis. The decreased abundance of a protein could suggest its targeting for degradation, such as via the proteasome pathway, or simply decreased expression. Confocal microscopy following immunofluorescence staining of the tubulins and tropomyosin revealed profound alterations in the microtubular network along with peripheralization of both α- and β-tubulins and tropomyosin staining. In addition, a subpopulation of paraptotic cells, likely corresponding to a more advanced stage of the cell death process, displayed a dramatic decrease in both α- and β-tubulin levels. The temporal and causal relationship, if any, between the disruption of the microtubular network observed in cells undergoing paraptosis and the formation of the cytoplasmic vacuoles remains to be established. The early disruption of the microtubular network observed here in paraptosis provides a distinguishing feature for this type of cell death as compared to type 2 or autophagic cell death as the current body of evidence concurs regarding a functional or at least a facilitating role for microtubules in the process of autophagy [see Monastyrska et al., 2009, for a review). Consequently, staining of tubulins along with already known autophagy markers could be envisioned as a potential tool to differentiate these two types of cell death.

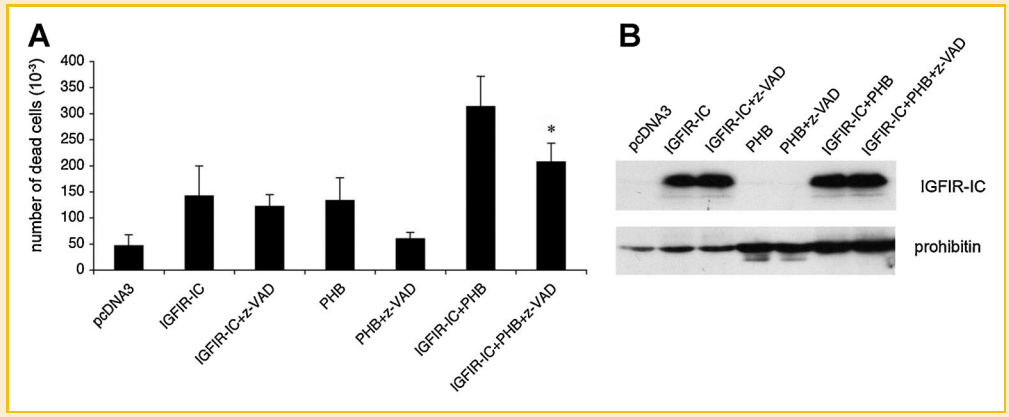

Fig. 8. Coexpression of IGF-IR-IC and prohibitin (PHB) potentiates paraptosis. A: 293T cells were transfected with the indicated constructs, and cell death was measured after 48 h. The error bars represent the SD of three independent experiments. The asterisk denotes a statistically significant difference with the sample IGF-IR-IC + z-VAD as assessed by Student's *t*-test ($P < 0.021$). B: Western blot analysis verifies the expression of the prohibitin and IGF-IR-IC constructs.

The overall decrease in PEBP levels during paraptosis that we observed in this study appears to play an important role in the execution of paraptosis. In fact, when we restored the levels of PEBP in cells undergoing paraptosis, by means of overexpression, the cell death induced by the IGF-IR-IC was prevented, and the activation of the JNK pathway suppressed.

This result is consistent with previous reports showing that a member of the PEBP family, hPEBP4, could prevent apoptosis induced by TNF-α by inhibiting the activation of the Raf-1/MEK/ERK and JNK pathways, and by preventing phopsphatidylethanolamine externalization [Wang et al., 2004a]. Taken together, these results indicate that PEBP may be an important survival factor capable of preventing cell death induced by multiple pathways. Though PEBP is known for its suppression of the MAPK pathway (which is also known to participate in paraptosis) through direct inhibition of the Raf kinase, its role as an inhibitor of paraptosis appears to be due to the suppression of the JNK rather than the MAPK pathway. As PEBP was shown to be a suppressor of the MAPK pathway through its specific inhibition of Raf, it is likely that a kinase distinct from Raf is responsible for the MEK/MAPK engagement in paraptosis. This result highlights the specificity of activating and inhibiting signals in different cell death pathways.

Interestingly, the possible involvement of PEBP in the pathogenesis of Alzheimer's disease has been proposed based on findings of decreased expression levels of the protein or its mRNA in the hippocampus of both AD patients [Maki et al., 2002] and the transgenic mouse model Tg2576, in which decreased PEBP expression correlated with accumulation of Aβ [George et al., 2006]. Though both groups see a possible link between lower levels of PEBP (that also functions as the precursor for the HCNP) and the neuronal dysfunction in AD, it is equally possible that a decline in the survival input by PEBP may play a role in AD pathogenesis by mediating a specific loss of neurons associated with AD.

We have investigated the potential importance of prohibitin in paraptosis, one of the first genes to be identified as up-regulated during pcd in unicellular organisms [Welburn and Murphy, 1998]. It has been reported that prohibitin enhances and regulates p53 activity and likely participates in decisions between proliferation and apoptosis [Fusaro et al., 2002]. Upon apoptotic stimulation, prohibitin translocates to mitochondria [Fusaro et al., 2002]. Our findings indicate that, in addition to the higher levels of prohibitin seen in cells undergoing paraptosis by SDS–PAGE Western blotting and immunocytochemistry, prohibitin synergizes with the IGFIR to induce a cell death that is only modestly inhibitable by caspase inhibitors; this could implicate a possible involvement of p53 in paraptosis that should be further investigated.

While some protein alterations associated with paraptosis were striking, such as those seen with prohibitin and ATP synthase, changes observed for others, such as some structural proteins, were less dramatic, although consistently reproduced. We cannot exclude the possibility that even modest alterations of some structural proteins might have a significant impact on cell organization and ultimately in the execution of paraptosis. On the other hand, it is possible that more dramatic alterations occur within a subpopulation of cells and/or in relation to a specific stage of the paraptotic program. This latter scenario was proven true at least for the alterations in the distribution and levels of the cytoskeletal proteins α- and β-tubulin where more and less dramatic differences are displayed in distinct subpopulations of cells transfected with the paraptosis-inducing expression construct IGF-IR-IC.

In conclusion, we report here the identification of several protein alterations that occur during paraptosis. Two of these represent new modulators of paraptosis. In our experiments, overexpressed prohibitin acted as an agonist, and PEBP as an antagonist, of paraptosis. The peculiar redistribution of α- and β-tubulin and tropomyosin observed in the early stages of paraptosis could be exploited as a defining feature of paraptosis in the effort to develop specific markers for this non-apoptotic cell death pathway, and to define its similarity or dissimilarity to the autophagic cell death program(s). Based on morphological criteria, we believe that paraptosis corresponds to type 3 pcd; however, a definite classification should follow the establishment of specific molecular markers. Cell death described as type 3 pcd and resembling paraptosis has been observed during development, primarily in the

nervous system [reviews in Clarke, 1990 and Sperandio and de Belle, 2008]. We believe that the characterization of paraptosis described here will help establish the occurrence of paraptosis during development. Increasing evidence indicates that at least part of the cell death found in some neurodegenerative diseases such as Huntington's disease and amyotrophic lateral sclerosis [Dal Canto and Gurney, 1994; Turmaine et al., 2000], and in other neurological conditions such as ischemic damage [Majno and Joris, 1995], is not apoptotic and, at least in some cases, resembles paraptosis at the morphological level. The identification of specific markers for paraptosis and other less well-characterized forms of cell death will be extremely useful in detecting and elucidating the progression of diseases and conditions involving cell death.

MATERIALS AND METHODS

CELL CULTURE, CONSTRUCTS, AND TRANSFECTIONS

Human embryonic kidney (HEK) 293T cells were cultured in DMEM (Mediatech, Inc., Herndon, VA) containing 10% FBS (Sigma, St. Louis, MO) and 100 U/ml penicillin/streptomycin (Mediatech, Inc.). The human insulin-like growth factor I receptor β subunit intracellular domain (IGF-IR-IC) was described previously [Sperandio et al., 2000]. The control vector pcDNA3 was obtained from Invitrogen (Carlsbad, CA). The human pcDNA3-PEBP construct was subcloned from an NT2 cell cDNA library. The human pcDNA3-prohibitin construct was obtained from the laboratory of Dr. S. Chellappan. For transfection, 3.5×10^6 cells were seeded into 10 cm plates. The following day, when cells were approximately 50–60% confluent, cells were transfected with 6 μg of either control pcDNA3 or pcDNA3-IGF-IR-IC using 30 μl of Lipofectamine 2000 (Invitrogen). At the time of transfection, fresh serum-containing media were added to the transfection mix. Floating and attached cells were harvested 48 h after transfection. Transfection efficiency, as estimated by cell rounding in IGFIR transfections, was typically 70–90%. Cell death was assessed in floating cells by trypan blue exclusion as described previously [Sperandio et al., 2000].

IMMUNOCYTOCHEMISTRY

HEK 293T cells that were stained with 250 nM Mitotracker Deep Red 633 according to the manufacturer's instructions (Molecular Probes, Inc., Eugene, OR) for 45 min. Cells were fixed in 4% PFA in PBS for 20 min at room temperature (RT) and then washed twice in PBS and once in TBS. For PEBP staining, cells were first fixed in methanol. Cells were permeabilized in 0.25% Triton in TBS for 10 min at RT and then washed twice in TBS. Blocking serum (5% NDS in TBS) was applied for 45 min followed by primary antibody diluted in 2.5% NDS in TBS overnight at 4°C. Primary antibodies included: anti-prohibitin (1:50, MS-261-P, NeoMarkers), anti-PEBP/RKIP (1:50, sc-5426, Santa Cruz Biotechnology), anti-IGF-IRβ (1:200–1:1,000, sc-713, Santa Cruz Biotechnology), anti-α-tubulin (4 μg/ml, sc-8035, Santa Cruz Biotechnology), anti-β-tubulin (1:100, T4026, Sigma), and anti-tropomyosin (gift). Three TBS washes were followed by incubation in secondary antibody for 45 min at RT (donkey anti-Ms IgG or donkey anti-Rb IgG with Alexa-fluor 488, 555, or 647 conjugates used at 1:250, 1:500, or 1:200, Molecular Probes, Inc.). Multiple stainings were performed serially overnight at 4°C, that is, IGF-IR followed by PEBP/RKIP. Mounting in Vectashield mounting medium (Vector Labs) followed three TBS washes. Images were acquired on a Nikon PCM-2000 confocal equipped with 488 argon, 543 HeNe, and 633 HeNe lasers mounted on an Eclipse E800 microscope.

SUBCELLULAR FRACTIONATION

For extract preparation, floating and adherent cells were collected from plates, spun, and washed twice with cold PBS. After one wash with hypotonic buffer HEB (50 mM PIPES, pH 7.3, 50 mM KCl, 5 mM EGTA, 2 mM $MgCl_2$), one volume of HEB containing Complete Mini protease inhibitor cocktail (Roche, Indianapolis, IN) was added to the cell pellet and the cell resuspension was incubated on ice for 1 h. Cells were dounce homogenized with 100 strokes of B pestle and spun at 3,000 rpm (1,000*g*) for 5 min producing a nuclear pellet (P1). The resulting supernatant was spun at 20,000*g* for 20 min to produce the heavy membrane/mitochondrial pellet (P20). This resulting supernatant was spun for 1 h at either 50,000 rpm (111,000*g*) to produce cytosol (S100) or at 100,000 rpm (446,000*g* r_{max}) to produce a pellet containing light membranes/microsomes (P400) and resulting cytosol (S400). Pellets were solubilized in Ready Prep Sequential Extraction Reagent 3 (Bio-Rad, Hercules, CA). Protein concentration was determined using a Bradford-based Coomassie Plus Protein Assay reagent (Pierce, Rockford, IL) using BSA as a standard.

1D SDS–PAGE AND WESTERN BLOT ANALYSIS

For 1D SDS–PAGE, typically 20 μg of cell extracts was run under reducing conditions on 10% NuPAGE Bis-Tris gels in MES buffer (Invitrogen) and transferred to PVDF membrane (Schleicher & Schuell Bioscience, Keene, NH). Western blots were performed in a solution of 5% nonfat dry milk in TBST. Following incubation with a species-specific HRP-conjugated secondary antibody (GE Healthcare, Piscataway, NJ) and ECL Western blotting detection reagents (GE Healthcare), proteins were detected by autoradiography. Quantitation of 1D SDS–PAGE Western blots was performed with a ChemiImager 4400 (Alpha Innotech, San Leandro, CA). Antibodies include: 14-3-3 β 1:200, phosphatidylethanolamine binding protein (RKIP) 1:200, α-tubulin 1:200, actin 1:200, enolase 1:200 (all from Santa Cruz Biotechnology), ATP synthase, subunit β 1:400 (Molecular Probes, Inc.), tropomyosin 1:100 (gift from Dr. Amy Sung), β-tubulin 1:500 (Sigma), prohibitin 1:200 (NeoMarkers), VCP 1:500 (BD, Franklin Lakes, NJ), P-MAPK, P-JNK, P-Jun, P-JNK, and JNK-1 (all at 1:1,000 from Cell Signaling), and IGFIR, β subunit 1:500 (Santa Cruz Biotechnology).

2D SDS–PAGE

Cell extracts (typically, 200–300 μg) were either dialyzed (if the sample was a supernatant) in 3500 MWCO dialysis cups (Pierce) against a buffer containing 8 M urea, 0.4% CHAPS, 0.04 M Tris base, 0.2% Biolytes 3-10 (Bio-Rad) and then brought to 2% CHAPS or directly dissolved in Bio-Rad Reagent 3 (if pellets). Samples were reduced with tributylphosphine (TBP, 10 μl/ml) for 20 min. A eleven-centimeter pH 3–10 IPG strips were hydrated with sample at 20°C for 12 h at 50 V using a Protean IEF cell (Bio-Rad). The strips were then focused for 35,000 V h. For the second dimension, strips

were incubated in 1.5 ml of buffer containing 6 M urea, 4% SDS, 20% glycerol, and 0.375 M Tris, pH 8.8, and 10 μl/ml TBP for 20 min and then run on 10–20% Tris–HCl Criterion gels (Bio-Rad) for 1 h at 200 V using Tris–glycine SDS running buffer. Gels were stained either with Fast Stain Colloidal Coomassie (Zoion Biotech, Shrewsbury, MA) and imaged with a GS710 densitometer (Bio-Rad) and/or first with SYPRO-Ruby (Invitrogen) and imaged with a Typhoon 8600 phosphoimager (GE Healthcare). Spot pattern differences between treatments were visualized directly and/or quantitated using PDQuest 7.1.0 software (Bio-Rad).

DIGE (2D FLUORESCENCE DIFFERENCE GEL ELECTROPHORESIS)

DIGE analysis (GE Healthcare) was performed to compare the abundance of specific proteins between experimental conditions within the same gel. The control extract was labeled with Cy3 (green) and the paraptotic extract with Cy5 (red). First, extracts were solubilized in Bio-Rad Reagent 3 and dialyzed separately in 10,000 MWCO cups for 2 h against 30 mM Tris, pH 8.8, 5 mM magnesium acetate, 8 M urea, and 0.4% CHAPS. Samples were brought to 4% CHAPS. Extracts (50 μg each) were then labeled with either 1 μl (400 pmol) of *N*-hydroxy succinimidyl (NHS) ester DIGE CyDye3 (Control) or CyDye5 (Paraptosis) on ice for 30 min in the dark, terminated by the addition of 10 nM lysine for 10 min on ice, combined, and brought to a final volume of 185 μl with Bio-Rad Ready Prep Sequential Extraction Reagent 2. The sample was subsequently reduced with 100 mM DTT for 20 min at RT, spun down, and loaded for IEF. 2D SDS–PAGE was performed as described above except that the strip was incubated in equilibration buffer containing 2% DTT for 10 min followed by buffer containing 2.5% iodoacetamide for an additional 10 min. After imaging with the Typhoon 8600, the differential spot intensities were analyzed by DeCyder 2D software (GE Healthcare). Multiple spots that were greater than 1.5-fold different between the two treatments were excised from the gel and identified by mass spectrometry.

IN-GEL PROTEOLYTIC DIGESTION OF PROTEINS

Protein spots of interest were manually excised from the gel and processed with an automatic in-gel digester Robot, ProGest (Genomic Solutions, Ann Arbor, MI). The gel spots were destained and dehydrated with acetonitrile. Subsequently, the proteins were reduced with 10 mM DTT at 60°C for 30 min, alkylated with 100 mM iodoacetamide at 37°C for 45 min, and then incubated with 125–250 ng trypsin at 37°C for 4 h. The resulting tryptic peptides were extracted from the gel either by using an organic extraction method (60% acetonitrile/5% formic acid) or by using an aqueous extraction method (10% formic acid), and then analyzed by mass spectrometry. Sequencing grade, modified trypsin (porcine) was purchased from Promega (Madison, WI), and iodoacetamide and DTT were obtained from Sigma.

MASS SPECTROMETRY

Mass spectra of digested protein gel spots were obtained by matrix-assisted laser desorption ionization time-of-flight (MALDI-TOF) mass spectrometry on a Voyager DESTR plus instrument (Applied Biosystems). Selected proteolytic peptide extracts were also analyzed by reverse-phase nano-HPLC–MS/MS with an Ultimate HPLC (Dionex) connected to a QSTAR Pulsar i quadrupole orthogonal TOF mass spectrometer (MDS Sciex) as previously described [Schilling et al., 2005; Schilling et al., 2006]. HPLC solvents such as acetonitrile and water were obtained from Burdick & Jackson (Muskegon, MI). For MALDI-MS experiments, a matrix solution of α-cyano-4-hydroxycinnamic acid in acetonitrile/methanol was purchased from Agilent Technologies (Palo Alto, CA).

BIOINFORMATICS AND PROTEIN DATABASE SEARCHES

Mass spectrometric data were analyzed with an in-house licensed bioinformatics database search engine Mascot (version 2.1) (Matrix Sciences, London, UK) [Perkins et al., 1999]. MALDI-MS data were first processed with Mascot Wizard version 1.1.2 (Matrix Sciences) and then submitted to the Mascot search engine. The MALDI-MS PMF data were matched against peptides from known protein sequences searching SwissProt (species: human) using the following parameters: 100 ppm mass accuracy, two missed proteolytic cleavages allowed (data were internally calibrated, i.e., using trypsin autolysis masses, such as m/z 842.5100 and 2211.1046). For ESI-MS/MS data sets, spectra were submitted using Mascot Daemon to our in-house Mascot server. Mascot uses a probability-based "Mowse Score" to evaluate data obtained from MS and MS/MS spectra, respectively. For a score >54 (probability $P<0.05$), protein matches are considered significant [Perkins et al., 1999].

ACKNOWLEDGMENTS

We thank Dr. Amy Sung for the anti-tropomyosin antibody, Dr. S. Chellappan for the human pcDNA3-prohibitin construct, Dr. Gurmil Gendeh from GE Healthcare Life Sciences for the DIGE analysis, Cathy Vitelli for assistance with confocal imaging, and Molly Anne Susag for manuscript preparation. This work was supported by a grant from the National Institutes of Health (AG12282 to D.E.B.).

REFERENCES

Ameisen JC. 2002. On the origin, evolution, and nature of programmed cell death: A timeline of four billion years. Cell Death Differ 9:367–393.

Castro-Obregon S, Del Rio G, Chen SF, Swanson RA, Frankowski H, Rao RV, Stoka V, Vesce S, Nicholls DG, Bredesen DE. 2002. A ligand–receptor pair that triggers a non-apoptotic form of programmed cell death. Cell Death Differ 9:807–817.

Chatellard-Causse C, Blot B, Cristina N, Torch S, Missotten M, Sadoul R. 2002. Alix (ALG-2-interacting protein X), a protein involved in apoptosis, binds to endophilins and induces cytoplasmic vacuolization. J Biol Chem 277:29108–29115.

Clarke PG. 1990. Developmental cell death: Morphological diversity and multiple mechanisms. Anat Embryol 181:195–213.

Dal Canto MC, Gurney ME. 1994. Development of central nervous system pathology in a murine transgenic model of human amyotrophic lateral sclerosis. Am J Pathol 145:1271–1279.

Fischer U, Janicke RU, Schulze-Osthoff K. 2003. Many cuts to ruin: A comprehensive update of caspase substrates. Cell Death Differ 10:76–100.

Fombonne J, Padron L, Enjalbert A, Krantic S, Torriglia A. 2006. A novel paraptosis pathway involving LEI/L-DNaseII for EGF-induced cell death in somato-lactotrope pituitary cells. Apoptosis 11:367–375.

Fusaro G, Wang S, Chellappan S. 2002. Differential regulation of Rb family proteins and prohibitin during camptothecin-induced apoptosis. Oncogene 21:4539–4548.

George AJ, Holsinger RM, McLean CA, Tan SS, Scott HS, Cardamone T, Cappai R, Masters CL, Li QX. 2006. Decreased phosphatidylethanolamine binding protein expression correlates with Abeta accumulation in the Tg2576 mouse model of Alzheimer's disease. Neurobiol Aging 27:614–623.

Gerner C, Frohwein U, Gotzmann J, Bayer E, Gelbmann D, Bursch W, Schulte-Hermann R. 2000. The Fas-induced apoptosis analyzed by high throughput proteome analysis. J Biol Chem 275:39018–39026.

Hengst U, Albrecht H, Hess D, Monard D. 2001. The phosphatidylethanolamine-binding protein is the prototype of a novel family of serine protease inhibitors. J Biol Chem 276:535–540.

Jadus MR, Chen Y, Boldaji MT, Delgado C, Sanchez R, Douglass T, Al-Atar U, Schulz W, Lloyd C, Wepsic HT. 2003. Human U251MG glioma cells expressing the membrane form of macrophage colony-stimulating factor (mM-CSF) are killed by human monocytes in vitro and are rejected within immunodeficient mice via paraptosis that is associated with increased expression of three different heat shock proteins. Cancer Gene Ther 10:411–420.

Majno G, Joris I. 1995. Apoptosis, oncosis, and necrosis. An overview of cell death. Am J Pathol 146:3–15.

Maki M, Matsukawa N, Yuasa H, Otsuka Y, Yamamoto T, Akatsu H, Okamoto T, Ueda R, Ojika K. 2002. Decreased expression of hippocampal cholinergic neurostimulating peptide precursor protein mRNA in the hippocampus in Alzheimer disease. J Neuropathol Exp Neurol 61:176–185.

Monastyrska I, Rieter E, Klionsky DJ, Reggiori F. 2009. Multiple roles of the cytoskeleton in autophagy. Biol Rev Camb Philos Soc 84:431–448.

Ojika K, Mitake S, Tohdoh N, Appel SH, Otsuka Y, Katada E, Matsukawa N. 2000. Hippocampal cholinergic neurostimulating peptides (HCNP). Prog Neurobiol 60:37–83.

Perkins DN, Pappin DJ, Creasy DM, Cottrell JS. 1999. Probability-based protein identification by searching sequence databases using mass spectrometry data. Electrophoresis 20:3551–3567.

Perry SV. 2001. Vertebrate tropomyosin: Distribution, properties and function. J Muscle Res Cell Motil 22:5–49.

Schilling B, Bharath MMS, Row RH, Murray J, Cusack MP, Capaldi RA, Freed CR, Prasad KN, Andersen JK, Gibson BW. 2005. Rapid purification and mass spectrometric characterization of mitochondrial NADH dehydrogenase (complex I) from rodent brain and a dopaminergic neuronal cell line. Mol Cell Proteomics 4:84–96.

Schilling B, Murray J, Yoo CB, Row RH, Cusack MP, Capaldi RA, Gibson BW. 2006. Proteomic analysis of succinate dehydrogenase and ubiquinol-cytochrome c reductase (complex II and III) isolated by immunoprecipitation from bovine and mouse heart mitochondria. Biochim Biophys Acta 1762:213–222.

Schneider D, Gerhardt E, Bock J, Muller MM, Wolburg H, Lang F, Schulz JB. 2004. Intracellular acidification by inhibition of the Na+/H+-exchanger leads to caspase-independent death of cerebellar granule neurons resembling paraptosis. Cell Death Differ 11:760–770.

Sperandio S, de Belle I. 2008. Paraptosis. In: Roninson IB, Brown MJ, Bredesen DE, editors. *Beyond apoptosis: Cellular outcomes of cancer therapy*. New York: Informa Healthcare. pp 157–174.

Sperandio S, de Belle I, Bredesen DE. 2000. An alternative, nonapoptotic form of programmed cell death. Proc Natl Acad Sci USA 97:14376–14381.

Sperandio S, Poksay K, De Belle I, Lafuente MJ, Liu B, Nasir J, Bredesen DE. 2004. Paraptosis: Mediation by MAP kinases and inhibition by AIP-1/Alix. Cell Death Differ 11:1066–1075.

Thiede B, Dimmler C, Siejak F, Rudel T. 2001. Predominant identification of RNA-binding proteins in Fas-induced apoptosis by proteome analysis. J Biol Chem 276:26044–26050.

Thompson WE, Branch A, Whittaker JA, Lyn D, Zilberstein M, Mayo KE, Thomas K. 2001. Characterization of prohibitin in a newly established rat ovarian granulosa cell line. Endocrinology 142:4076–4085.

Turmaine M, Raza A, Mahal A, Mangiarini L, Bates GP, Davies SW. 2000. Nonapoptotic neurodegeneration in a transgenic mouse model of Huntington's disease. Proc Natl Acad Sci USA 97:8093–8097.

Wang X, Li N, Liu B, Sun H, Chen T, Li H, Qiu J, Zhang L, Wan T, Cao X. 2004a. A novel human phosphatidylethanolamine-binding protein resists tumor necrosis factor alpha-induced apoptosis by inhibiting mitogen-activated protein kinase pathway activation and phosphatidylethanolamine externalization. J Biol Chem 279:45855–45864.

Wang Y, Li X, Wang L, Ding P, Zhang Y, Han W, Ma D. 2004b. An alternative form of paraptosis-like cell death, triggered by TAJ/TROY and enhanced by PDCD5 overexpression. J Cell Sci 117:1525–1532.

Welburn SC, Murphy NB. 1998. Prohibitin and RACK homologues are upregulated in trypanosomes induced to undergo apoptosis and in naturally occurring terminally differentiated forms. Cell Death Differ 5:615–622.

Yeung K, Seitz T, Li S, Janosch P, McFerran B, Kaiser C, Fee F, Katsanakis KD, Rose DW, Mischak H, Sedivy JM, Kolch W. 1999. Suppression of Raf-1 kinase activity and MAP kinase signalling by RKIP. Nature 401:173–177.

Yuan J, Horvitz HR. 1992. The *Caenorhabditis elegans* cell death gene ced-4 encodes a novel protein and is expressed during the period of extensive programmed cell death. Development 116:309–320.

Yuan J, Shaham S, Ledoux S, Ellis HM, Horvitz HR. 1993. The *C. elegans* cell death gene ced-3 encodes a protein similar to mammalian interleukin-1 beta-converting enzyme. Cell 75:641–652.